Solid-State Phosphine Ligand Engineering via Postsynthetic Modification of Amine-Functionalized MOFs

Aidan F. Greene, Jiehye Shin, and Casey R. Wade*

Department of Chemistry and Biochemistry, The Ohio State University, Columbus, Ohio 43210, United States

ABSTRACT: Postsynthetic phospha-Mannich condensation has been investigated for the design of solid-state phosphine ligands using amine-functionalized metal-organic frameworks (MOFs). Hydroxymethylphosphine precursors $Ph_2P(CH_2OH)$, $PhP(CH_2OH)_2$, and $CyP(CH_2OH)_2$ readily condense at the 2-aminoterephthalate linkers of MIL-101(Al)-NH_2 and IRMOF-3 to generate the phosphine-functionalized MOFs **MIL/IRMOF-PPh$_2$-*x*, MIL/IRMOF-PPh-*x*,** and **MIL/IRMOF-PCy-*x***, respectively, where *x* denotes phosphine loading per amine site. Solution-state ^{1}H and ^{31}P{^{1}H} NMR spectra of base-digested MOFs reveal that $PhP(CH_2OH)_2$ and $CyP(CH_2OH)_2$ react at the amine groups of adjacent linkers, resulting in intra-framework cross-linking. The phosphinated MOFs have been investigated as solid-state ligands for Ir-catalyzed C–H borylation of arenes. **MIL-PPh-0.1** and **MIL-PCy-0.1** exhibit good activity for the benchmark C–H borylation of toluene when metalated with $[Ir(OMe)(cod)]_2$ (cod = 1,5-cyclooctadiene). **MIL-PPh$_2$-0.1** and the IRMOF-3 derivatives show little or no catalytic turnover under the same conditions, revealing that phosphine connectivity and MOF topology and pore size are critical factors in solid-state ligand design.

INTRODUCTION

The ubiquity of phosphine ligands in transition metal catalysis has prompted efforts to integrate them into heterogeneous supports as a means of improving catalyst stability, activity, and recyclability.[1–4] Recently, metal-organic frameworks (MOFs) have emerged as promising platforms for the design of solid-state phosphine ligands. There have been several reported examples of MOFs assembled from linkers based on central phosphine groups that provide structural support.[5–16] MOFs constructed from linkers with pendent phosphines that are not structural components have also been reported.[17–21] However, these materials have typically relied on direct synthesis approaches that suffer from disadvantages such as phosphine oxidation during solvothermal synthesis, high ligand site density, and a lack of control over the topology and porosity of the resulting MOF.

Postsynthetic modification (PSM) has become an indispensable means of tuning the properties and reactivity of MOFs.[22–25] Covalent modification of MOF linkers bearing functional groups such as amines, alkynes, azides, or aldehydes has been used to introduce a wide range of different functional groups that are not compatible with direct synthesis methods. It has also been applied for intra-framework cross-linking.[26–28] For example, Sada reported postsynthetic cross-linking of a Zn MOF containing azide-functionalized linkers via click reaction with a tetraalkyne.[29] Similarly, Devic and Clet showed that thermolysis of UiO-66-COOH promotes intra-framework cross-linking via formation of anhydride bridges.[30]

PSM routes for phosphine functionalization of pre-synthesized MOFs can obviate some of the disadvantages of direct synthesis, but remain quite rare.[31] Solvent-assisted ligand incorporation (SALI) has been used to append triarylphosphines containing carboxylate and sulfonate functional groups at the nodes of MOF-808.[32,33] The resulting materials were subject to postsynthetic metalation with Rh or Ir and investigated as catalysts for reductive amination and alkene hydroformylation. Phosphine-containing MOFs have also recently been prepared by PSM of amine-functionalized linkers using imine condensation and amide coupling reactions.[34,35]

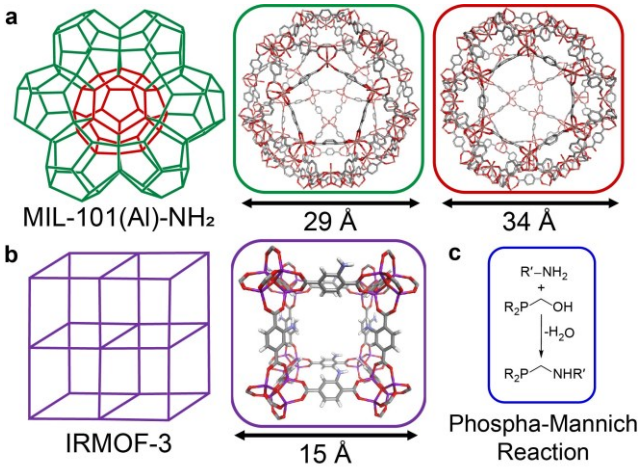

Figure 1: Framework and pore structures of a) MIL-101(Al)-NH_2 and b) IRMOF-3. c) Generic phospha-Mannich condensation reaction.

Herein, we describe the implementation of postsynthetic phospha-Mannich reactions as a rapid and convenient means of covalently appending phosphine ligands in amine-functionalized MOFs. Phospha-Mannich reactions have been well-studied for homogeneous ligand design and utilize hydroxymethyl phosphine groups as point of condensation with nucleophilic amines.[36]

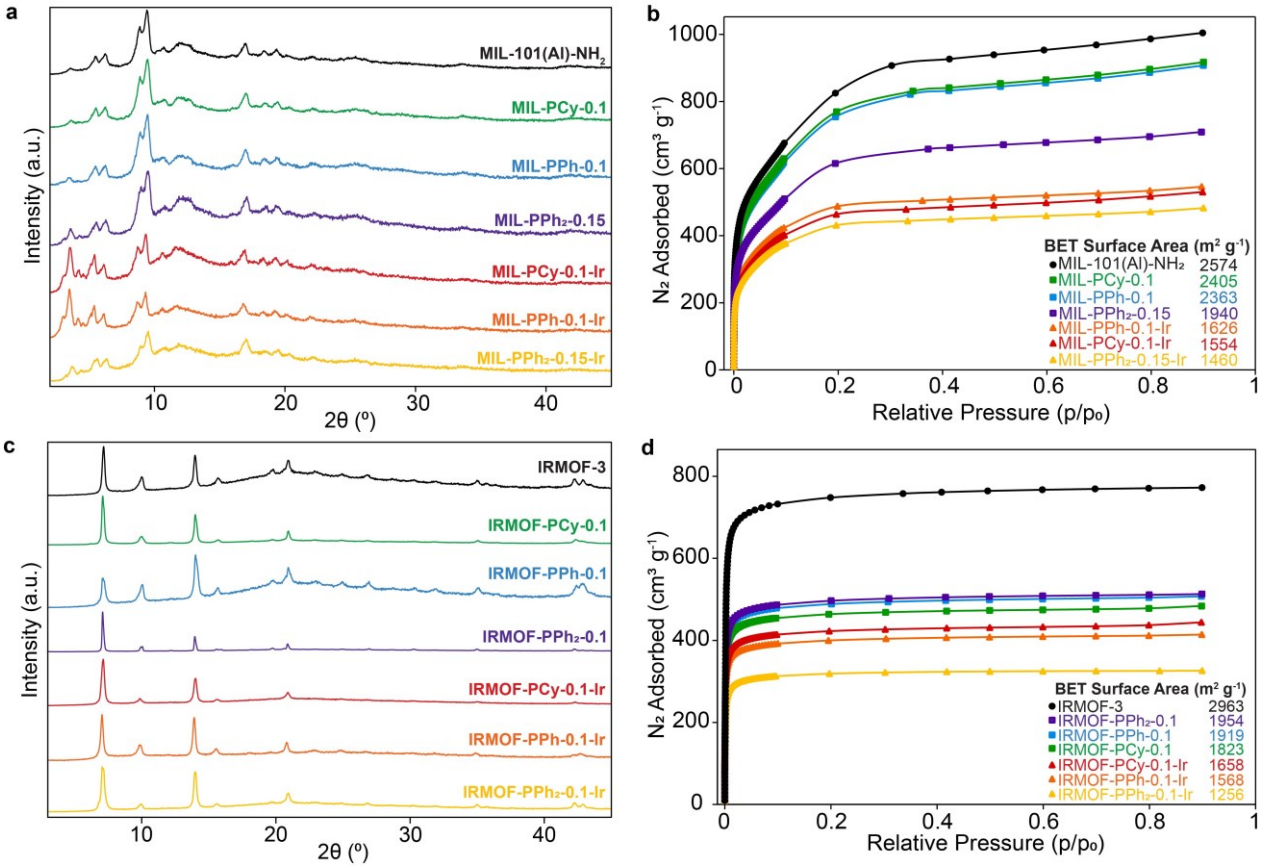

Figure 2. a) PXRD patterns and b) N_2 adsorption isotherms (77 K) with calculated BET surface areas for **MIL-PR-0.1-Ir**, **MIL-PR-0.1**, **MIL-PPh$_2$-0.15**, and MIL-101(Al)-NH$_2$. c) PXRD patterns and d) N_2 adsorption isotherms (77 K) with calculated BET surface areas for **IRMOF-PR-0.1-Ir**, **IRMOF-PR-0.1**, **IRMOF-PPh$_2$-0.1**, and IRMOF-3.

In the present work, the phosphine precursors $Ph_2P(CH_2OH)$, $PhP(CH_2OH)_2$, and $CyP(CH_2OH)_2$ have been found to readily condense with amine-functionalized terephthalate linkers in MIL-101(Al)-NH$_2$ and IRMOF-3 to provide solid-state phosphine ligands with controllable loadings (Figure 1). Notably, the *bis*(hydroxymethyl)phosphine precursors result in intra-framework cross-linking at low phosphine loadings. The phosphinated MOFs have been investigated as solid-state ligands for Ir-catalyzed C–H borylation of arenes.[37,38] Solid-state ^{31}P NMR studies and catalytic screening results reveal that MIL-101(Al)-NH$_2$ supports catalytically active Ir-phosphine species while pore diameter or pore window size limitations prevent the formation of analogous species in IRMOF-3. Additionally, bridging phosphine ligands associated with intra-framework cross-linking are found to be more effective at supporting catalytically active Ir species than pendent phosphine groups.

RESULTS AND DISCUSSION

The phosphine-functionalized MOFs **MIL/IRMOF-PPh$_2$-*x*, MIL/IRMOF-PPh-*x*,** and **MIL/IRMOF-PCy-*x*** were prepared by treating MIL-101(Al)-NH$_2$ or IRMOF-3 with acetonitrile solutions of the hydroxymethylphosphine precursors $Ph_2P(CH_2OH)$, $PhP(CH_2OH)_2$, and $CyP(CH_2OH)_2$, respectively (Scheme 1). Here, *x* denotes equivalents of phosphine precursor per MOF amine site used in the postsynthetic modification reactions. Powder X-ray diffraction (PXRD) analysis confirms that the MOFs retain crystallinity following the postsynthetic phosphination reactions (Figure 2a,c). N_2 adsorption isotherms also show that N_2-accessible porosity is maintained and BET surface areas decrease with increased phosphine loading (Figure 2b,d and Figure S1).

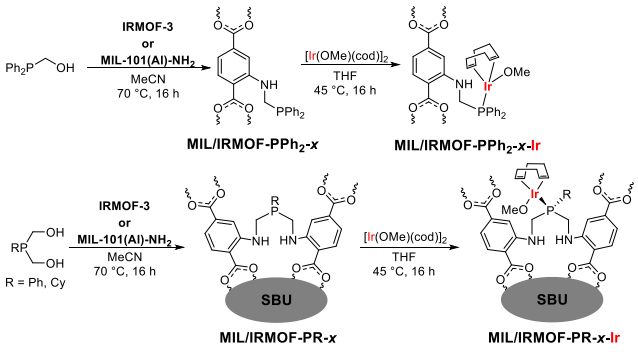

Scheme 1: Postsynthetic phosphination and metalation of amine-functionalized MOFs using different phosphine precursors.

Solution-state ^{1}H and ^{31}P{^{1}H} NMR analysis of base-digested MOF samples was used to characterize the modified linkers and quantify the extent of phosphine incorporation. The ^{31}P{^{1}H} NMR spectra of the **MIL-PPh$_2$-*x*** and **IRMOF-PPh$_2$-*x*** derivatives show the formation of a single phosphine species around -22 ppm, which is consistent with an independently prepared homogeneous analogue $Ph_2P(CH_2NH\text{-}bdc^{Me})$ (-18 ppm, $NH_2\text{-}bdc^{Me}$ = dimethyl aminoterephthalate, Figure S2-4). The base-digested ^{1}H NMR spectra exhibit all expected resonances for the new phosphine-functionalized linkers as well as

unreacted NH_2-bdc linkers (Figures S5-S7). Integration of the **MIL-PPh$_2$-*x*** spectra reveals that the postsynthetic modification reactions are nearly quantitative for x = 0.15-0.80, corresponding to the general empirical formula $Al_3O(Cl)(NH_2\text{-bdc})_{3-3x}(Ph_2PCH_2NH\text{-bdc})_{3x}$ (NH_2-bdc = 2-aminoterephthalate). Greater batch-to-batch variability was observed for phosphine loadings below x = 0.15, while x = 0.80 was consistently observed as a saturation limit even with the use of excess $Ph_2P(CH_2OH)$. For **IRMOF-PPh$_2$-*x***, phosphine loadings of x = 0.1-0.30 gave quantitative reactions according to the general formula $Zn_4O(NH_2\text{-bdc})_{3-3x}(Ph_2PCH_2NH\text{-bdc})_{3x}$. Attempts to prepare **IRMOF-PPh$_2$-*x*** at higher loadings revealed x = 0.3-0.4 as the saturation limit. The maximum phosphine loadings observed for **MIL-PPh$_2$-*x*** and **IRMOF-PPh$_2$-*x*** are consistent with the differences in accessible pore volume for the two MOFs.[39,40]

The short distances between amine groups of adjacent linkers coordinated to the secondary building units (SBUs) of MIL-101(Al)-NH_2 and IRMOF-3 are well-suited to accommodate intra-framework cross-linking by the $PhP(CH_2OH)_2$ and $CyP(CH_2OH)_2$ phosphine precursors (Scheme 1). Accordingly, solution-state ^{1}H and ^{31}P{^{1}H} NMR data for the base-digested **MIL/IRMOF-PR-*x*** derivatives clearly indicate formation of phosphine-bridged linker species corresponding to empirical formulas of $Al_3O(Cl)(NH_2\text{-bdc})_{3-6x}[RP(CH_2NH\text{-bdc})_2]_{3x}$ and $Zn_4O(NH_2\text{-bdc})_{3-6x}[RP(CH_2NH\text{-bdc})_2]_{3x}$. The ^{31}P{^{1}H} NMR spectra of the PCy and PPh MOF derivatives exhibit resonances around -23 and -32 ppm, respectively, which are consistent with those observed for independently prepared $RP(CH_2NH\text{-bdc}^{Me})_2$ homogeneous analogues (Figures S8-9). The digested ^{1}H NMR spectra also display the expected resonances for phosphine-bridged linker species and support nearly quantitative reaction of $PhP(CH_2OH)_2$ and $CyP(CH_2OH)_2$ with the NH_2-bdc linkers up to $x \approx 0.30$ (Figures S10-17). However, at loadings of $x \geq 0.30$, the spectra show appearance of a new species corresponding to the hydroxymethyl phosphine groups with a singly appended linker (i.e. $RP(CH_2OH)(CH_2NH\text{-bdc})$) (Figures S8-9). The incomplete condensation reaction reflects a critical density limit for cross-linking adjacent linkers that corresponds to ~60 % functionalization and the presence of a phosphine group in alternating pores.

Solid-state ^{31}P NMR spectra were also measured to corroborate the base-digested data. **MIL-PPh$_2$-0.33** and **IRMOF-PPh$_2$-0.1** each show a major phosphine resonance around -15 ppm commensurate with the solution-state data (Figure S27). **IRMOF-PPh-0.3** gives rise to a single major resonance at -14 ppm while **IRMOF-PCy-0.3** exhibits two phosphine resonances at -5 and -21 ppm (Figure S28-29). These signals are shifted slightly downfield with respect to those observed in the solution-state spectra but remain consistent with the presence of unoxidized phosphine groups. On the other hand, **MIL-PPh-0.3** and **MIL-PCy-0.3** exhibit a series of broad resonances that span the 0 to -40 ppm range, indicating the presence of multiple distinct phosphine species (Figure S28-29).[5] Additional signals in the +15 to +40 ppm region are attributed to oxidized phosphine groups resulting from air exposure during sample preparation and data collection. The MIL-101(Al)-NH_2 framework includes hexagonal and pentagonal windows connecting the large mesoporous cages as well as small trigonal windows that are part of the super tetrahedron building blocks.[41] Each of these windows contains adjacent amine-functionalized linkers capable of supporting the bridging phosphine groups (Figure S37). Consequently, the multiple phosphine species observed in the solid-state NMR spectra of **MIL-PPh-0.3** and **MIL-PCy-0.3** most likely arise from the different microenvironments presented by these windows. This explanation is further supported by the ^{31}P{^{1}H} NMR spectra for the digested MOFs which only show the presence of a single phosphine species in solution.

Lin and co-workers have shown that a Zr MOF assembled from triarylphosphine-based linkers could be postsynthetically metalated with $[Ir(OMe)(cod)]_2$ (cod = 1,5-cyclooctadiene), resulting in a material with excellent catalytic activity for C–H borylation of arenes.[9] The MOF catalyst exhibited up to 840 turnovers for borylation of benzene with B_2pin_2 under neat conditions, which greatly surpassed the activity of a homogeneous analogue. Solid-state monophosphine ligands supported on silica have also shown good activity for Ir-catalyzed C–H borylation of arenes.[42–45] These reports motivated us to investigate the phosphinated MIL-101(Al)-NH_2 and IRMOF-3 frameworks as solid-state ligands for Ir-based C–H borylation and gain insight into how the method of phosphine immobilization influences catalytic activity and product selectivity.

Table 1. Catalytic C–H borylation of toluene.[a]

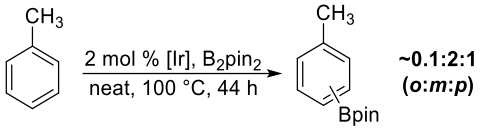

Entry	Catalyst [Ir]	TON[b] R = Ph	TON[b] R = Cy
1	IRMOF-PR$_2$-0.1-Ir	< 5	-
2	IRMOF-PR-0.1-Ir	< 5	< 5
3	MIL-PR$_2$-0.15-Ir	< 5	-
4	MIL-PR-0.1-Ir	87(±6)[e]	86(±3)[e]
5[c]	MIL-PR-0.1-Ir (cyclohexane)	-	9
6[c]	MIL-PR-0.1-Ir (dioxane)	-	< 5
7	MIL-PR-0.1-IrCl	80	81
8	MIL-PR-0.1-Ir (0.2 mol %)	38	63
9[d]	$RP(CH_2NH\text{-}BDC^{Me})_2$ + 0.5 $[Ir(OMe)(cod)]_2$	< 5	7
10[d]	PR_3 + 0.5 $[Ir(OMe)(cod)]_2$	63	93
11	MIL-101(Al)-NH_2 + $[Ir(OMe)(cod)]_2$	< 5	

[a]Reaction conditions: B_2pin_2 (66 mM), catalyst (0.0013 mmol Ir), toluene (2 mL), 44 h, 100 °C. [b]Turnover numbers (TON) are reported as total borylated products per Ir. TONs were determined by GC-FID with respect to an internal standard (hexamethylbenzene). See Experimental Section for additional details. [c]Reactions were carried out in the indicated solvent with an initial toluene concentration of 528 mM. [d]Reactions were carried out using the standard conditions but with a 0.5:1 ratio of $[Ir(OMe)(cod)]_2$ to phosphine. [e]The TONs are reported as an average and standard deviation of three reactions using different batches of fresh MOF catalyst.

Activated samples of the low-loading phosphinated MOFs (x = 0.1-0.15) were suspended in THF and treated with 0.5 equiv. of $[Ir(OMe)(cod)]_2$ per phosphine group to generate **MIL-PPh$_2$-0.15-Ir**, **MIL-PPh-0.1-Ir**, **MIL-PCy-0.1-Ir**, **IRMOF-PPh$_2$-0.1-Ir**, **IRMOF-PPh-0.1-Ir**, and **IRMOF-PCy-0.1-Ir**. During the postsynthetic metalation reactions, the yellow color of the supernatant solutions gradually dissipated concomitant with subtle color changes of the solid MOFs. PXRD analysis confirmed that the MOFs retain crystallinity after the metalation reactions, and N_2 gas adsorption isotherms show a pronounced decrease in BET surface area relative to the parent materials (Figure 2b,d). Unlike the parent phosphinated MOFs, the Ir-metalated materials do not cleanly depolymerize under basic digestion conditions, and as a result no discernable signals were observed in the solution-state $^{31}P\{^1H\}$ NMR spectra. Nevertheless, the solid-state ^{31}P NMR spectra of **MIL-PPh$_2$-0.33-Ir**, **MIL-PPh-0.1-Ir**, and **MIL-PCy-0.1-Ir** show clear downfield shifts of the broad phosphine resonances to around +10 ppm (Figures S30-32), which closely match the chemical shifts of the homogeneous ligands upon metalation with $[Ir(OMe)(cod)]_2$ and $[IrCl(cod)]_2$ (Figures S18-26). Inductively coupled plasma optical emission spectroscopy (ICP-OES) analysis of the MIL-101(Al)-NH_2 derivatives supports nearly quantitative metalation of the phosphine sites (Table S1). In contrast, the solid-state ^{31}P NMR spectra of **IRMOF-PPh$_2$-0.1-Ir**, **IRMOF-PPh-0.1-Ir**, and **IRMOF-PCy-0.1-Ir** are unchanged compared to those obtained prior to metalation (Figures S33-35). The absence of new downfield shifted resonances indicates that P–Ir species are not formed. However, X-ray fluorescence spectroscopy (XRF) data and decreased BET surface areas support adsorption of Ir in the frameworks (Figure S38 and Table S2).

Optimized model structures of **MIL-PPh-*x*** and **IRMOF-PPh-*x*** were examined in an attempt to understand their contrasting behavior toward metalation (Figures S36-37) The percent buried volume around the phosphine sites was calculated to gauge their accessibility for complexation of the Ir(OMe)(cod) species.[46,47] In **IRMOF-PPh-*x***, the bridging phosphine ligands are confined to the corners of the cubic pores, resulting in a buried volume of 36.6 % for a sphere radius of 3.5 Å. This value is larger than that reported for PPh_3 (29.6 %) but smaller than for the more sterically hindered P(*o*-Tol)$_3$ (41.1 %).[48] Expanding the sphere radius to 5.0 Å results in only a modest increase to 41.1 % buried volume for **IRMOF-PPh-*x***. The mesoporous cages in MIL-101(Al)-NH_2 contain hexagonal, pentagonal, and trigonal windows with adjacent linkers that are potentially suitable for accommodating the bridging phosphine groups. All three possibilities were evaluated, giving calculated buried volumes of 35.4 %, 40.2 %, and 36.1 %, respectively, for a sphere radius of 3.5 Å. The similarity in buried volumes for **MIL-PPh-*x*** and **IRMOF-PPh-*x*** suggest that phosphine sites in both materials should be capable of accommodating the Ir(OMe)(cod) fragment. However, they may not reflect the space required for complexation of the Ir species. In this regard, the large mesoporous cages of MIL-101(Al)-NH_2 should be more accommodating of the ligand substitution reaction involving $[Ir(OMe)(cod)]_2$ or Ir(OMe)(cod)(THF) species. Moreover, the smaller pore windows in IRMOF-3 (< 8 Å) compared to MIL-101(Al)-NH_2 (12-16 Å) likely hinder transport of the Ir precursor species to the phosphine sites.[49] Consequently, although the local steric profile around the phosphine sites in **IRMOF-PPh-*x*** does not provide a definitive explanation for its recalcitrance toward metalation, MOF topology, pore diameter, and pore window size are still likely be causal factors.

Toluene was used as a benchmark substrate for screening the catalytic C–H borylation activity of the Ir-metalated MOFs. Reactions were performed in neat toluene at 100 °C with 2 mol % Ir catalyst and *bis*(pinacolato)diboron (B_2pin_2, 66 mM) as the borylating reagent. The B_2pin_2 concentration was based on initial reaction optimization. The IRMOF-3 derivatives (Table 1, entries 1-2) exhibited < 5 turnover numbers (TONs) per Ir after 44 h. This low activity is comparable to that observed in a control reaction with a mixture of the parent MIL-101(Al)-NH_2 and $[Ir(OMe)(cod)]_2$ (Table 1, entry 11), confirming that phosphine ligation is necessary to support the Ir-based active species. Unexpectedly, **MIL-PPh$_2$-0.15-Ir** also exhibits low catalytic activity (Table 1, entry 3). PXRD analysis showed that the catalytically inactive MOFs retain crystallinity after reaction screening, indicating that framework collapse is not responsible for the poor turnover (Figures S39-40). However, all of the inactive MOFs quickly darkened in color upon heating under the catalytic reaction conditions, suggesting rapid degradation of the Ir species. In contrast, **MIL-PPh-0.1-Ir** and **MIL-PCy-0.1-Ir** gave average TONs of 87(±6) and 86(±3) per Ir, respectively, after 44 h (Table 1, entry 4). The high TONs in excess of 50 reveal consumption of B_2pin_2 and continued turnover with the HBpin byproduct as the borylating reagent.[50,51] The isomer ratio of the borylated toluene products (~2:1 *meta*:*para*) is consistent with the statistical distribution expected for substrate-controlled regioselectivity. These initial screening results indicate that the linker-bridging phosphine ligands support catalytically active Ir species while the pendent $–CH_2PPh_2$ ligands are prone to degradation. The small difference in TONs observed for **MIL-PPh-0.1-Ir** and **MIL-PCy-0.1-Ir** further suggests that the identity of the phosphine substituent (i.e. Ph versus Cy) does not have a strong influence on catalytic activity.

A hot filtration test with **MIL-PCy-0.1-Ir** showed an abrupt halt of catalytic activity when the solid MOF was removed from the reaction after ~10 turnovers (Figure S41), supporting the heterogeneous nature of the catalyst. Many homogeneous iridium catalysts have shown good activity with dilute arene substrates, prompting us to screen **MIL-PCy-0.1-Ir** with 0.5 M solutions of toluene in cyclohexane or dioxane (Table 1, entries 5 and 6). Unfortunately, a dramatic decrease in catalyst activity was observed in both solvents. The pronounced concentration effect can be attributed to hindered substrate diffusion and has been observed for other MOF-supported arene borylation catalysts.[52] When $[IrCl(cod)]_2$ was used as the metalating reagent instead of $[Ir(OMe)(cod)]_2$, the resulting MOFs **MIL-PPh-0.1-IrCl** and **MIL-PCy-0.1-IrCl** gave slightly lower TONs after 44 h (Table 1, entry 7). The modest decrease in activity using the Ir–Cl precatalyst species is consistent with previous reports.[50,51]

Unfortunately, the **MIL-PR-0.1-Ir** catalysts could not be effectively recycled. They showed significantly decreased activity when isolated by filtration after 20 h and resubjected to the C–H borylation reaction conditions (Figure S42). This behavior suggests decomposition of the catalytically-active Ir species in the absence of B_2pin_2 and/or arene substrate. Consistent with this notion, catalytic turnover was maintained when the toluene borylation reactions were sequentially spiked with an additional 50 equiv. of B_2pin_2 after 20 h and 40 h (Figure S43). With the cumulative addition of 150 equiv. of B_2pin_2, the MOF catalysts gave TONs of 150 and 182 for R = Ph and Cy, respectively after 108 h. However, lower overall yields (100 % for R = Ph and

121 % for R = Cy) compared to the standard reaction conditions (182 % for R = Ph and 190 % for R = Cy after 44 h) point to gradual degradation of the catalytically active Ir species over long reaction times. In addition, experiments carried out with low catalyst loadings of 0.2 mol % Ir resulted in modestly decreased TONs after 44 h (Table 1, entry 8).

Table 2. Catalytic C–H borylation of mono-substituted arenes using MIL-PR-0.1-Ir catalysts.[a]

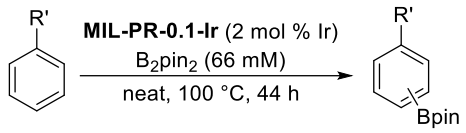

Entry	Substrate R' =	TON[b] R = Ph	TON[b] R = Cy	Prod. Dist. (*o*:*m*:*p*)
1	Me	87(±6)	86(±3)	3:61:36
2	Et	81	78	1:66:33
3	*i*Pr	71	76	0:67:33
4	*t*Bu	43	59	0:66:34
5	$SiMe_3$	15	10	0:67:33
6	F	89	98	36:45:19
7	C(O)OEt	69	74	27:50:23
8	OMe	92	96	12:56:32
9	NMe_2	< 5	< 5	-

[a]Reaction conditions: B_2pin_2 (66 mM), catalyst (0.0013 mmol Ir), toluene, 44 h, 100 °C. [b]Turnover numbers (TON) are reported as total borylated products per Ir site. TONs were determined by GC-FID with respect to an internal standard (hexamethylbenzene). See Supporting Information for additional details.

Lastly, we sought to compare the catalytic activity of **MIL-PPh-0.1-Ir** and **MIL-PCy-0.1-Ir** with precatalysts prepared *in situ* using related homogeneous phosphine ligands and $[Ir(OMe)(cod)]_2$. The analogous aminomethyl phosphine ligands $PhP(CH_2NH\text{-}bdc^{Me})_2$ and $CyP(CH_2NH\text{-}bdc^{Me})_2$ exhibited poor catalytic activity, yielding 4 and 7 TON, respectively (Table 1, entry 9). In contrast, commercially available PPh_3 and PCy_3 gave comparable activity to the MOF catalysts, yielding 63 and 93 turnovers, respectively (Table 1, entry 10). Attempts to obtain kinetic profiles of the catalytic borylation reactions with **MIL-PPh-0.1-Ir** and **MIL-PCy-0.1-Ir** for comparison with the homogeneous phosphine ligands have been complicated by batch-to-batch variability (Figure S44). Large variations in the catalyst induction periods (1-4 h) and apparent rates have been observed irrespective of the MOF parentage. Notably, Farha and co-workers have reported observing similar batch-to-batch variability in their study of UiO-67-based catalysts for C–H borylation of arenes.[52]

MIL-PPh-0.1-Ir and **MIL-PCy-0.1-Ir** were subsequently screened wtih a small library of mono-substituted arenes to probe for size exclusion effects and the potential influence of MOF microenvironment on product regioselectivity. Increasing the size of the alkyl substituent from Me to Et to *i*Pr resulted in modest decreases in the catalyst TON (Table 2, entries 1-3), but a precipitous drop in activity was observed for tert-butylbenzene and trimethylsilylbenzene (Table 2, entries 4-5). In all cases, statistical ~2:1 *meta*:*para* product distributions are observed. These results suggest that sterically encumbering substituents negatively impact substrate diffusion to the active site, but there is no unexpected product regioselectivity indicative of steric crowding around the catalyst. Substrates with polar functional groups including fluorobenzene, ethylbenzoate, and anisole (Table 2, entries 6-8) yielded good TONs and an increase in the fraction of the *ortho*-borylated products owing to directing group effects.[53,54] The presence of the strongly electron-donating amine group in dimethyl aniline (Table 2, entry 9) resulted very low substrate conversion, consistent with previous reports for Ir diphosphine and bipyridine catalysts.[51] Overall, the MOF-based catalysts exhibit compatibility with electron withdrawing functional groups but show pronounced decreases in activity with increasing substrate size. Moreover, the product regioselectivities indicate that the MOF microenvironment does not influence substrate C–H activation at the catalyst sites.

CONCLUSIONS

MIL-101(Al)-NH_2 and IRMOF-3 are found to accommodate up to 0.8 and 0.3 pendent $–CH_2PPh_2$ groups per amine site, respectively, using Ph_2PCH_2OH as a phosphine precursor. The disparity in the upper limits of phosphine functionalization is attributed to the difference in pore sizes of the two MOFs. Owing to the proximity of the amine groups on adjacent linkers coordinated at the MOF SBUs, intra-framework cross-linking is observed when *bis*(hydroxymethyl)phosphine precursors are employed at low loadings (< 0.3 per amine site). After postsynthetic metalation with $[Ir(OMe)(cod)]_2$, solid-state ^{31}P NMR data corroborate the formation of Ir phosphine species in **MIL-PPh_2-0.1-Ir**, **MIL-PPh-0.1-Ir**, and **MIL-PCy-0.1-Ir**. However, ^{31}P NMR spectra reveal that the phosphine groups remain uncoordinated in the IRMOF-3 derivatives. Percent buried volume calculations indicate that the local steric environments around the phosphine sites in **IRMOF-PPh-*x*** and **MIL-PPh-*x*** are surprisingly similar, and both should be able to accommodate coordination of the Ir(OMe)(cod) fragments. This leads us to postulate that MOF topology, pore diameter, and pore aperture size have a more nuanced effect on the postsynthetic metalation reaction. In line with the absence of phosphine supported Ir catalyst species, the phosphinated IRMOF-3 derivatives showed little or no activity as solid-state ligands for C–H borylation of toluene. On the other hand, phosphine cross-linked **MIL-PPh-0.1-Ir** and **MIL-PCy-0.1-Ir** exhibit comparable activity to homogeneous PPh_3 and PCy_3 ligands, yielding >90 TON for the benchmark C–H borylation of toluene. No catalytic turnover was observed for **MIL-PPh_2-0.1-Ir**, containing pendent $–CH_2PPh_2$ groups, indicating that increased connectivity imparts stability to the phosphine ligands. **MIL-PPh-0.1-Ir** and **MIL-PCy-0.1-Ir** proved to be competent catalysts for a range of small arenes substrates. However, decreased catalytic activity was observed with increasing substrate size, and the MOF microenvironment did not influence product regioselectivity.

Although PSM has been used to design MOFs with a wide variety of functional groups, methods for the introduction of phosphine ligands have remained scarce.[31–35] Here, we have shown that phospha-Mannich reactions can be used to append phosphine ligands at the amine sites of MIL-101(Al)-NH_2 and IRMOF-3. This PSM strategy is complementary to direct

synthesis approaches, which have been more commonly employed for the design of phosphine-functionalized MOFs. It allows for the use of MOFs with pre-determined structures and pore sizes while also providing control over phosphine loading. Moreover, the hydroxymethylphosphine precursors are easily prepared from commercially-available primary or secondary phosphines, offering the ability to tune steric and electronic properties of the resulting phosphine ligands. Altogether, the postsynthetic phospha-Mannich reaction offers new opportunities for the design of solid-state ligand platforms to support heterogenous transition metal catalysts.

EXPERIMENTAL SECTION

General Considerations. All manipulations were carried out using a nitrogen-filled glovebox unless otherwise noted. Acetonitrile, tetrahydrofuran, toluene, and fluorobenzene were degassed by sparging with ultra-high purity argon and passed through columns of drying agents using a Pure Process Technologies solvent purification system. IRMOF-3,[55] $[Ir(OMe)(cod)]_2$,[56] and dimethyl 2-aminoterephthalate[57] were prepared according to literature procedures. $AlCl_3 \cdot 6H_2O$ (Ward's Science), 2-aminoterephthalic acid (Thermo Scientific), and DMF (Fisher Chemical) were used as received for the preparation MIL-101(Al)-NH_2. Phenylphosphine (Beantown Chemical), cyclohexylphosphine (STREM), bis(pinacolato)diboron (Frontier Scientific), and pinacolborane (TCI America) were used as received and stored at -20 °C in an N_2-filled glovebox. Hexamethylbenzene was purchased from TCI America and dried prior to use. All arene substrates were purchased from commercial suppliers and dried and distilled prior to use.

Powder X-ray diffraction patterns were measured using a Rigaku Miniflex 600 diffractometer with nickel-filtered Cu Kα radiation (λ = 1.5418 A). XRF spectroscopic data for were obtained using an Innov-X Systems X-5000 spectrometer with a 50 keV, 10 W Tantalum X-ray tube. Additional details about the XRF measurements can be found in the Supporting Information. N_2 (77 K) gas adsorption measurements were performed using a Micromeritics 3Flex Surface Characterization Analyzer with ultrahigh-purity N_2 (Praxair, NI 5.0UH-K). Prior to analysis, samples (100-200 mg) were transferred to oven-dried and tared sample tubes equipped with TranSeals™ (Micrometrics). The samples were heated to 100 °C (MIL(Al)-101-NH_2 and IRMOF-3), 60 °C (MIL/IRMOF-PR/PPh_2-*x*), or 45 °C (MIL/IRMOF-PR/PPh_2-*x*-Ir) at initial ramp rate of 1 °C min^{-1} under vacuum until the outgas rate was less than 0.0033 mbar min^{-1}. BET surface areas were calculated from the N_2 adsorption isotherms by fitting the data to the BET equation using the 3-Flex software package (v5.02, Micromeritics). The appropriate pressure range for the fitting ($0.0001 \leq P/Po \leq 0.1$) was determined by the consistency criteria of Rouquerol.[58,59]

Solution-state NMR spectra were measured using a Bruker DPX 400 or 600 MHz spectrometer. For ^1H NMR spectra, the solvent resonance was referenced as an internal standard. For $^{31}P\{^1H\}$ NMR spectra, 85% H_3PO_4 was used as an external standard (0 ppm). MOF samples were digested for solution-state NMR analysis by mixing 5-10 mg of MOF with ~5 mg of CsF and 5 drops of D_2O. Deuterated dimethyl sulfoxide (DMSO-d_6, 0.7 mL) was then added to provide a lock signal for shimming, and the mixture was sonicated until homogeneous. Solvent-suppressed ^1H NMR spectra were collected using a 180° water selective excitation sculpting with default parameters and pulse shapes. Spectra were collected using selective pulses of 1 ms with the transmitter frequency set to the center of the solvent resonance.

Solid-state NMR experiments were performed using a Bruker Avance III HD Ascend 600 MHz NMR spectrometer equipped with a triple-resonance (HXY) DNP probe that was operated in dual-mode ^1H-^{31}P at a resonance frequency of 243 MHz for ^{31}P. Samples were packed into 3.2 mm ZrO_2 rotors inside an N_2-filled glovebox. Experiments were carried out at magic angle spinning frequencies of 15 kHz at room temperature. Quantitative multi-CP experiments were acquired with total CP-durations of 11 ms, comprised of 0.1 ms pulses. Recycle delays were set from 2-3 s and spectra were acquired with 12k scans. Chemical shifts were externally calibrated to triphenylphosphine (-6 ppm).

Elemental microanalyses (C, H, N) were performed by Robertson Microlit Laboratories (Ledgewood, NJ). ICP-OES analyses (P, Ir) were conducted by the Trace Element Research Laboratory at The Ohio State University (Columbus, OH).

Synthesis of MIL-101(Al)-NH_2. MIL-101(Al)-NH_2 was synthesized following a slightly modified literature procedure.[60] Briefly, 2-aminoterephtalic acid (1.09 g, 6.0 mmol) was dissolved in 240 mL of DMF and heated to 110 °C in an oil bath. Solid $AlCl_3 \cdot 6H_2O$ (2.9 g, 12.0 mmol) was added in 14 equal portions (~200 mg each) every 15 minutes with slow stirring. Following the final addition, the reaction mixture was stirred slowly for an additional 3 h, and then left overnight without stirring at 110 °C. The resulting solid was filtered and washed with DMF (60 mL) and ethanol (60 mL) before being subjected to Soxhlet extraction with ethanol for 24 h. The solid was then filtered and washed with additional ethanol (20 mL) and dried *in vacuo* at 100 °C for 12 hours. Digested ^1H NMR (600 MHz, CsF/D_2O/DMSO-d_6): δ 7.56 (d, 1H, $^3J_{H-H}$ = 8.21 Hz), 7.02 (s, 1H), 6.88 (dd, 1H, $^3J_{H-H}$ = 8.21 Hz, $^4J_{H-H}$ = 1.21 Hz)

Synthesis of hydroxymethyldiphenylphosphine ($Ph_2P(CH_2OH)$), *bis*(hydroxymethyl)phenylphosphine ($PhP(CH_2OH)_2$) and *bis*(hydroxymethyl)cyclohexylphosphine ($CyP(CH_2OH)_2$). The hydroxymethyl phosphine precursors were prepared according to the following general procedure adapted from the literature.[61] A 20 mL scintillation vial was charged with paraformaldehyde (0.546 g, 18.2 mmol). The corresponding phosphine (Ph_2PH: 2.0 g, 18.2 mmol; $PhPH_2$: 1.0 g, 9.1 mmol; $CyPH_2$: 1.06 g, 9.1 mmol) was added, and the reaction mixture was heated at 100 °C for 1 h with rapid stirring to yield a colorless oil. After cooling to room temperature, the oily products were triturated with pentane (10 mL) multiple times until a crystalline solid was formed. The solids were dried *in vacuo* to provide the corresponding hydroxymethyl phosphines in 75-85 % yield. The NMR spectroscopic data below are consistent with that reported in the literature.

$Ph_2P(CH_2OH)$: ^1H NMR (400 MHz, $CDCl_3$): δ 7.50 (m, 4H), 7.37 (m, 6H), 4.42 (m, 2H), 1.45 (m, 1H); $^{31}P\{^1H\}$ NMR (162 MHz, $CDCl_3$): δ -9.1 (s); **$PhP(CH_2OH)_2$:** ^1H NMR (400 MHz, $CDCl_3$): δ 7.63 (m, 2H), 7.40 (m, 3H), 4.48 (m, 4H), 2.69 (m, 2H); $^{31}P\{^1H\}$ NMR (162 MHz, $CDCl_3$): δ -14.8 (s); **$CyP(CH_2OH)_2$:** ^1H NMR (400 MHz, $CDCl_3$): δ 4.26 (m, 4H), 3.18 (m, 4H), 2.35 (m, 2H), 1.81 (m, 5H), 1.31 (m, 5H); $^{31}P\{^1H\}$ NMR (162 MHz, $CDCl_3$): Cy: δ -11.4 (s).

Postsynthetic phosphination of MIL-101(Al)-NH_2 and IRMOF-3 with $Ph_2P(CH_2OH)$, $PhP(CH_2OH)_2$, or $CyP(CH_2OH)_2$. Activated samples of MIL-101(Al)-NH_2 (0.20 g, 0.30 mmol) or IRMOF-3 (0.15 g, 0.18 mmol) were transferred to a 20 mL scintillation vial and suspended in anhydrous

acetonitrile (10 mL). A 0.1 M stock solution of the corresponding phosphine precursor was prepared in acetonitrile and the desired amount (0.1-1.0 equiv. per amine site) was added to the MOF suspension. This mixture was gently stirred at 70 °C overnight. The supernatant was decanted, and the solid product was washed with acetonitrile (3 × 10 mL) before being dried *in vacuo*. The phosphinated MOFs were then activated at 60 °C under vacuum for 12 h prior to gas adsorption measurements and metalation.

Metalation of MIL/IRMOF-PPh$_2$-*x*, MIL/IRMOF-PPh-*x*, and MIL/IRMOF-PCy-*x* with [Ir(OMe)(cod)]$_2$ or [IrCl(cod)]$_2$ An activated sample of the phosphinated MOF (0.15 g) was transferred to a 20 mL scintillation vial and suspended in THF (10 mL). A 0.1 M stock solution of [Ir(OMe)(cod)]$_2$ or [IrCl(cod)]$_2$ was prepared in THF, and an amount corresponding to 1 equiv. of Ir per phosphine was added to the MOF suspension. The mixture was gently stirred at 45 °C for 12 h, resulting in a slow dissipation of the yellow color from the supernatant solution. The colorless supernatant was then decanted, and the solid was washed with THF (3 × 10 mL) before being dried *in vacuo*. The metalated MOFs were activated at 45 °C under vacuum for 12 h prior to gas adsorption measurements and catalysis.

Synthesis of Homogeneous Phosphine Analogues Ph$_2$P(CH$_2$NH-bdc^{Me}), PhP(CH$_2$NH-bdc^{Me})$_2$, and CyP(CH$_2$NH-bdc^{Me})$_2$. A 20 mL scintillation vial was charged with dimethyl 2-aminoterephthalate (50 mg, 0.23 mmol) and dissolved in benzene (5 mL) with slight heating. A solution of the corresponding hydroxymethyl phosphine precursor (0.23 mmol of Ph$_2$P(CH$_2$OH) or 0.12 mmol of PhP(CH$_2$OH)$_2$/CyP(CH$_2$OH)$_2$) in benzene (2 mL) was then added to the vial. A catalytic amount of tosylic acid (<1 mg) was added to the reaction mixture. The vial was sealed and the reaction mixture was stirred at 80 °C for 12 h. The reaction progress was monitored in situ by ^{31}P{^{1}H} NMR spectroscopy to ensure full conversion of the starting material. The solvent was subsequently evaporated in vacuo to give the crude product as a dark yellow residue.

For **Ph$_2$P(CH$_2$NH-bdc^{Me})**, the crude product was lyophilized from benzene to produce a light yellow solid. The solid was washed with cold pentane (3 × 5 mL) and dried *in vacuo* to yield a light yellow solid (80 % yield). ^{1}H NMR (400 MHz, C_6D_6): δ 8.39 (br s, 1H), 7.95 (d, 1H, $^3J_{H-H}$ = 8.30 Hz), 7.83 (d, 1H, $^4J_{H-H}$ = 1.62 Hz), 7.43 (dd, 1H, $^3J_{H-H}$ = 8.30 Hz, $^4J_{H-H}$ = 1.62 Hz), 7.41 (m, 4H), 7.04 (m, 6H), 3.76 (t, 2H), 3.48 (s, 3H), 3.27 (s, 3H); ^{31}P{^{1}H} NMR (162 MHz, C_6D_6): δ -18.1 (s)

For **PhP(CH$_2$NH-bdc^{Me})$_2$**, the crude product was dissolved in diethyl ether (4 mL), and pentane (8 mL) was added. The mixture was then placed in a -20 °C freezer for 1 h, resulting in precipitation of a very pale yellow solid. The solid was collected by filtration, washed with cold pentane (3 × 5 mL), and dried *in vacuo* to yield the product as a light yellow solid (50 % yield). ^{1}H NMR (400 MHz, C_6D_6): δ 8.27 (br s, 2H), 7.93 (d, 2H, $^3J_{H-H}$ = 8.25 Hz), 7.73 (d, 2H, $^4J_{H-H}$ = 1.64 Hz), 7.42 (dd, 2H, $^3J_{H-H}$ = 8.25 Hz, $^4J_{H-H}$ = 1.64 Hz), 7.39 (m, 2H), 7.07 (m, 3H), 3.50 (m, 4H), 3.49 (s, 6H), 3.33 (s, 6H); ^{31}P{^{1}H} NMR (162 MHz, C_6D_6): δ - 28.4 (s)

For **CyP(CH$_2$NH-bdc^{Me})$_2$**, the crude product was washed with pentane (3 × 5 mL) to remove a dark yellow impurity, dissolved in diethyl ether (6 mL), and placed in a -20 °C freezer for 1 h resulting in precipitation of an light yellow solid. The solid was collected by filtration, washed with cold pentane (3 × 5 mL) and dried *in vacuo* to yield a light yellow solid (60 % yield). ^{1}H NMR (400 MHz, C_6D_6): δ 8.32 (br s, 2H), 7.96 (d, 2H, $^3J_{H-H}$ = 8.23 Hz), 7.74 (d, 2H, $^4J_{H-H}$ = 1.53 Hz), 7.43 (dd, 2H, $^3J_{H-H}$ = 8.23 Hz, $^4J_{H-H}$ = 1.53 Hz), 3.49 (s, 6H), 3.38 (s, 6H), 3.33 (m, 4H), 1.77-1.47 (m, 5H), 1.28-1.02 (m, 6H); ^{31}P{^{1}H} NMR (162 MHz, C_6D_6): δ -20.5 (s)

Metalation of Homogeneous Phosphine Analogues with [Ir(OMe)(cod)]$_2$ or [IrCl(cod)]$_2$. A 20 mL scintillation vial was charged with Ph$_2$PCH$_2$NH-bdc^{Me}, PhP(CH$_2$NH-bdc^{Me})$_2$, or CyP(CH$_2$NH-bdc^{Me})$_2$ (0.05 mmol) and dissolved in CH_2Cl_2 (2 mL). A solution of [Ir(OMe)(cod)]$_2$ or [IrCl(cod)]$_2$ (0.025 mmol) in CH_2Cl_2 (1 mL) was added to the vial, causing an immediate color change from light yellow to dark red-brown. The reaction mixture was stirred at room temperature and monitored by in situ ^{31}P{^{1}H} NMR spectroscopy to ensure complete conversion of the starting materials. The solvent was removed *in vacuo* and the resulting products were characterized without further purification.

Catalytic Borylation of Neat Arene Substrates. In a typical procedure, stock solutions of hexamethylbenzene (200 mM, internal standard) and B_2pin_2 (200 mM) were prepared in the arene substrate. Using a syringe, 0.66 mL of each stock solution was transferred to a 1-dram vial along with 0.68 mL arene substrate to reach a total volume of 2 mL and B_2pin_2 concentration of 66 mM. This mixture was then transferred to a 1-dram vial containing the MOF or homogeneous catalyst (2 mol % iridium with respect to B_2pin_2), and the vials were sealed with a Teflon-lined screw cap. The reaction mixtures were stirred at 100 °C for 20-44 h. Aliquots of the reaction mixtures (10 μL) were removed at varying time points, diluted with CH_2Cl_2, filtered over Celite, and characterized by GC-FID. Turnover numbers per Ir were calculated using response factors (RF) determined by using quantitative ^{1}H NMR spectroscopy and GC-FID for authentic samples of the borylated products (see Figure S62 for additional details).

Catalytic Borylation of Toluene in Cyclohexane or Dioxane Solvent. Stock solutions of hexamethylbenzene (200 mM, internal standard) and B_2pin_2 (200 mM) were prepared in cyclohexane or dioxane. Using a syringe, 0.66 mL of each stock solution was transferred to a 1-dram vial along with 0.12 toluene substrate and 0.56 mL solvent to reach a total volume of 2 mL. The final concentrations were 528 mM toluene, and 66 mM B_2pin_2. The solutions were then transferred to a 1-dram vial containing the MOF catalyst (4-6 mg, 2 mol % iridium with respect to B_2pin_2), and the vials were sealed with a Teflon-lined screw cap. The reaction mixtures were stirred at 100 °C for 44 h. Aliquots of the reaction mixtures (10 μL) were removed at varying time points, diluted with CH_2Cl_2, filtered over Celite, and characterized by GC-FID.

Recyclability studies. A 1-dram vial was charged with **MIL-PCy-0.1-Ir** (2 mol % Ir), and the borylation reaction was prepared as described in the typical procedure. After 20 h, an aliquot (10 μL) of the reaction mixture was removed for GC-FID analysis, and the MOF catalyst was separated by filtration through a 0.45 μm PTFE syringe filter. The MOF was washed with toluene (3 × 3 mL) before being resubjected to identical catalytic reaction conditions as described above. (Figure S42)

Catalyst lifetime studies. A 1-dram vial was charged with **MIL-PCy-0.1-Ir** (2 mol % Ir), and the borylation reaction was prepared as described in the typical procedure. After 20 h, an aliquot (10 μL) was removed for GC-FID analysis. An additional 50 equivalents of B_2pin_2 was immediately added to the

reaction mixture, which was then left to stir for an additional 20 h. This process was repeated, after which the reaction was continued for a total of 108 h. (Figure S43)

Hot filtration test. Two identical reactions were prepared following the typical procedure for the catalytic borylation of toluene under neat conditions as described above. **MIL-PCy-0.1-Ir** (2 mol % Ir) was used as the catalyst and the reactions were heated at 80 °C. After 11 h (~20% yield, 10 TON), the MOF catalyst was removed from one of the reaction vials by filtration through a 0.45 μm PTFE syringe filter. The resulting solution was transferred to a clean 1-dram vial, sealed with a Teflon-lined cap, and heated at 80 °C. No further substrate conversion or product formation was observed after the hot filtration (Figure S41).

Control reaction with MIL-101(Al)-NH_2 and [Ir(OMe)(cod)]$_2$. MIL-101(Al)-NH_2 (0.021 g, 0.03 mmol) was suspended in THF (6 mL) in a 20 mL scintillation vial. [Ir(OMe)(cod)]$_2$ (0.030 g, 0.05 mmol) was dissolved in THF (~2 mL) and added to the MOF suspension. The resulting mixture was gently stirred at 45 °C overnight. After cooling to room temperature, the supernatant was decanted and the resulting solid was dried *in vacuo*. This material was then screened as a catalyst for toluene borylation according to the procedure described above. During the catalytic reaction, dark black particles formed in the reaction solution immediately upon heating, indicated the presence of iridium nanoparticles. No formation of borylated toluene products was observed by GC-FID (Table 1, entry 11).

Supporting Information

The Supporting Information is available free of charge on the ACS Publications website.

Solution- and solid-state NMR spectral data, XRF data, analytical data, gas adsorption isotherms and data, PXRD data, GC-FID chromatograms, additional experimental details (PDF)

Model structure coordinates (TXT)

AUTHOR INFORMATION

Corresponding Author

* Email: wade.521@osu.edu

Notes

The authors declare no competing financial interest.

ACKNOWLEDGMENTS

Acknowledgment is made to the National Science Foundation under Grant No. CHE-2044904 for support of this research. This study made use of the Campus Chemical Instrument Center NMR facility at Ohio State University. The authors also thank the Ohio Supercomputer Center for computational resources.[62]

REFERENCES

(1) Gäumann, P.; Cartagenova, D.; Ranocchiari, M. Phosphine-Functionalized Porous Materials for Catalytic Organic Synthesis. *European J Org Chem* **2022**, *2022* (48), e202201006. https://doi.org/10.1002/ejoc.202201006.

(2) Orton, G. R. F.; Pilgrim, B. S.; Champness, N. R. The Chemistry of Phosphines in Constrained, Well-Defined Microenvironments. *Chem Soc Rev* **2021**, *50* (7), 4411–4431. https://doi.org/10.1039/D0CS01556C.

(3) Landis, C. R.; Clark, T. P. Solid-Phase Synthesis of Chiral 3,4-Diazaphospholanes and Their Application to Catalytic Asymmetric Allylic Alkylation. *Proceedings of the National Academy of Sciences* **2004**, *101* (15), 5428–5432. https://doi.org/10.1073/pnas.0307572100.

(4) Yang, Y.; Beele, B.; Blümel, J. Easily Immobilized Di- and Tetraphosphine Linkers: Rigid Scaffolds That Prevent Interactions of Metal Complexes with Oxide Supports. *J Am Chem Soc* **2008**, *130* (12), 3771–3773. https://doi.org/10.1021/ja800541c.

(5) Humphrey, S. M.; Allan, P. K.; Oungoulian, S. E.; Ironside, M. S.; Wise, E. R. Metal–Organophosphine and Metal–Organophosphonium Frameworks with Layered Honeycomb-like Structures. *Dalton Transactions* **2009**, 2298–2305. https://doi.org/10.1039/b820038f.

(6) Nuñez, A. J.; Shear, L. N.; Dahal, N.; Ibarra, I. A.; Yoon, J.; Hwang, Y. K.; Chang, J.-S.; Humphrey, S. M. A Coordination Polymer of (Ph3P)AuCl Prepared by Post-Synthetic Modification and Its Application in 1-Hexene/n-Hexane Separation. *Chemical Communications* **2011**, *47* (43), 11855–11857. https://doi.org/10.1039/c1cc14682c.

(7) Václavík, J.; Servalli, M.; Lothschütz, C.; Szlachetko, J.; Ranocchiari, M.; van Bokhoven, J. A. Au(I) Catalysis on a Coordination Polymer: A Solid Porous Ligand with Free Phosphine Sites. *ChemCatChem* **2013**, *5* (3), 692–696. https://doi.org/10.1002/cctc.201200844.

(8) Nuñez, A. J.; Chang, M. S.; Ibarra, I. A.; Humphrey, S. M. Tuning the Host–Guest Interactions in a Phosphine Coordination Polymer through Different Types of Post-Synthetic Modification. *Inorg Chem* **2014**, *53* (1), 282–288. https://doi.org/10.1021/ic4022239.

(9) Sawano, T.; Lin, Z.; Boures, D.; An, B.; Wang, C.; Lin, W. Metal–Organic Frameworks Stabilize Mono(Phosphine)–Metal Complexes for Broad-Scope Catalytic Reactions. *J Am Chem Soc* **2016**, *138* (31), 9783–9786. https://doi.org/10.1021/jacs.6b06239.

(10) Bezrukov, A. A.; Törnroos, K. W.; Dietzel, P. D. C. Modification of Network and Pore Dimensionality in Metal–Organic Frameworks Containing a Secondary Phosphine Functionality. *Cryst Growth Des* **2017**, *17* (6), 3257–3266. https://doi.org/10.1021/acs.cgd.7b00243.

(11) Bezrukov, A. A.; Dietzel, P. D. C. A Permanently Porous Yttrium–Organic Framework Based on an Extended Tridentate Phosphine Containing Linker. *Inorg Chem* **2017**, *56* (21), 12830–12838. https://doi.org/10.1021/acs.inorgchem.7b01574.

(12) Dunning, S. G.; Nandra, G.; Conn, A. D.; Chai, W.; Sikma, R. E.; Lee, J. S.; Kunal, P.; Reynolds, J. E.; Chang, J.; Steiner, A.; Henkelman, G.; Humphrey, S. M. A Metal–Organic Framework with Cooperative Phosphines That Permit Post-Synthetic Installation of Open Metal Sites. *Angewandte Chemie International Edition* **2018**, *57* (30), 9295–9299. https://doi.org/10.1002/anie.201802402.

(13) Reynolds, J. E.; Walsh, K. M.; Li, B.; Kunal, P.; Chen, B.; Humphrey, S. M. Highly Selective Room Temperature Acetylene Sorption by an Unusual Triacetylenic Phosphine MOF. *Chemical Communications* **2018**, *54* (71), 9937–9940. https://doi.org/10.1039/C8CC05402A.

(14) Dunning, S. G.; Reynolds, J. E.; Walsh, K. M.; Kristek, D. J.; Lynch, V. M.; Kunal, P.; Humphrey, S. M. Direct, One-Pot Syntheses of MOFs Decorated with Low-Valent Metal-Phosphine Complexes. *Organometallics* **2019**, *38* (18), 3406–3411. https://doi.org/10.1021/acs.organomet.9b00319.

(15) Newar, R.; Begum, W.; Akhtar, N.; Antil, N.; Chauhan, M.; Kumar, A.; Gupta, P.; Malik, J.; Balendra; Manna, K. Mono-Phosphine Metal-Organic Framework-Supported Cobalt Catalyst for Efficient Borylation Reactions. *Eur J Inorg Chem*

2022, *2022* (10), e202101019. https://doi.org/10.1002/ejic.202101019.
(16) Chen, J.; Li, H.; Wang, H.; Song, Y.; Hong, Q.; Chang, K.; Hu, H.; Zhang, S.; Cao, L.; Wang, C. Phosphine-Based Metal–Organic Layers to Construct Single-Site Heterogeneous Catalysts for Arene Borylation. *Chemical Communications* **2023**, *59* (54), 8432–8435. https://doi.org/10.1039/D3CC01858J.
(17) Morel, F. L.; Ranocchiari, M.; van Bokhoven, J. A. Synthesis and Characterization of Phosphine-Functionalized Metal–Organic Frameworks Based on MOF-5 and MIL-101 Topologies. *Ind Eng Chem Res* **2014**, *53* (22), 9120–9127. https://doi.org/10.1021/ie403549v.
(18) Falkowski, J. M.; Sawano, T.; Zhang, T.; Tsun, G.; Chen, Y.; Lockard, J. V; Lin, W. Privileged Phosphine-Based Metal-Organic Frameworks for Broad-Scope Asymmetric Catalysis. *J Am Chem Soc* **2014**, *136* (14), 5213–5216. https://doi.org/10.1021/ja500090y.
(19) Xu, X.; Rummelt, S. M.; Morel, F. L.; Ranocchiari, M.; van Bokhoven, J. A. Selective Catalytic Behavior of a Phosphine-Tagged Metal-Organic Framework Organocatalyst. *Chemistry – A European Journal* **2014**, *20* (47), 15467–15472. https://doi.org/10.1002/chem.201404498.
(20) Morel, F. L.; Pin, S.; Huthwelker, T.; Ranocchiari, M.; van Bokhoven, J. A. Phosphine and Phosphine Oxide Groups in Metal–Organic Frameworks Detected by P K-Edge XAS. *Physical Chemistry Chemical Physics* **2015**, *17* (5), 3326–3331. https://doi.org/10.1039/C4CP05151C.
(21) Beloqui Redondo, A.; Morel, F. L.; Ranocchiari, M.; van Bokhoven, J. A. Functionalized Ruthenium–Phosphine Metal–Organic Framework for Continuous Vapor-Phase Dehydrogenation of Formic Acid. *ACS Catal* **2015**, *5* (12), 7099–7103. https://doi.org/10.1021/acscatal.5b01987.
(22) Cohen, S. M. Postsynthetic Methods for the Functionalization of Metal–Organic Frameworks. *Chem Rev* **2012**, *112* (2), 970–1000. https://doi.org/10.1021/cr200179u.
(23) Cohen, S. M. The Postsynthetic Renaissance in Porous Solids. *J Am Chem Soc* **2017**, *139* (8), 2855–2863. https://doi.org/10.1021/jacs.6b11259.
(24) Yin, Z.; Wan, S.; Yang, J.; Kurmoo, M.; Zeng, M. H. Recent Advances in Post-Synthetic Modification of Metal–Organic Frameworks: New Types and Tandem Reactions. *Coord Chem Rev* **2019**, *378*, 500–512. https://doi.org/10.1016/j.ccr.2017.11.015.
(25) Mandal, S.; Natarajan, S.; Mani, P.; Pankajakshan, A. Post-Synthetic Modification of Metal–Organic Frameworks Toward Applications. *Adv Funct Mater* **2021**, *31* (4), 2006291. https://doi.org/10.1002/adfm.202006291.
(26) Zhang, Y.; Feng, X.; Li, H.; Chen, Y.; Zhao, J.; Wang, S.; Wang, L.; Wang, B. Photoinduced Postsynthetic Polymerization of a Metal–Organic Framework toward a Flexible Stand-Alone Membrane. *Angewandte Chemie International Edition* **2015**, *54* (14), 4259–4263. https://doi.org/10.1002/anie.201500207.
(27) Furukawa, Y.; Ishiwata, T.; Sugikawa, K.; Kokado, K.; Sada, K. Nano- and Microsized Cubic Gel Particles from Cyclodextrin Metal–Organic Frameworks. *Angewandte Chemie International Edition* **2012**, *51* (42), 10566–10569. https://doi.org/10.1002/anie.201204919.
(28) Kalaj, M.; Cohen, S. M. Postsynthetic Modification: An Enabling Technology for the Advancement of Metal–Organic Frameworks. *ACS Cent Sci* **2020**, *6* (7), 1046–1057. https://doi.org/10.1021/acscentsci.0c00690.
(29) Ishiwata, T.; Furukawa, Y.; Sugikawa, K.; Kokado, K.; Sada, K. Transformation of Metal–Organic Framework to Polymer Gel by Cross-Linking the Organic Ligands Preorganized in Metal–Organic Framework. *J Am Chem Soc* **2013**, *135* (14), 5427–5432. https://doi.org/10.1021/ja3125614.
(30) Ragon, F.; Campo, B.; Yang, Q.; Martineau, C.; Wiersum, A. D.; Lago, A.; Guillerm, V.; Hemsley, C.; Eubank, J. F.; Vishnuvarthan, M.; Taulelle, F.; Horcajada, P.; Vimont, A.; Llewellyn, P. L.; Daturi, M.; Devautour-Vinot, S.; Maurin, G.; Serre, C.; Devic, T.; Clet, G. Acid-Functionalized UiO-66(Zr) MOFs and Their Evolution after Intra-Framework Cross-Linking: Structural Features and Sorption Properties. *J Mater Chem A Mater* **2015**, *3* (7), 3294–3309. https://doi.org/10.1039/C4TA03992K.
(31) Goesten, M. G.; Sai Sankar Gupta, K. B.; Ramos-Fernandez, E. V.; Khajavi, H.; Gascon, J.; Kapteijn, F. Chloromethylation as a Functionalisation Pathway for Metal–Organic Frameworks. *CrystEngComm* **2012**, *14* (12), 4109. https://doi.org/10.1039/c2ce06594k.
(32) Prasad, R. R. R.; Dawson, D. M.; Cox, P. A.; Ashbrook, S. E.; Wright, P. A.; Clarke, M. L. A Bifunctional MOF Catalyst Containing Metal–Phosphine and Lewis Acidic Active Sites. *Chemistry – A European Journal* **2018**, *24* (57), 15309–15318. https://doi.org/10.1002/chem.201803094.
(33) Samanta, P.; Solé-Daura, A.; Rajapaksha, R.; Wisser, F. M.; Meunier, F.; Schuurman, Y.; Sassoye, C.; Mellot-Draznieks, C.; Canivet, J. Heterogenized Molecular Rhodium Phosphine Catalysts within Metal–Organic Frameworks for Alkene Hydroformylation. *ACS Catal* **2023**, *13* (7), 4193–4204. https://doi.org/10.1021/acscatal.3c00398.
(34) Wu, Y.; Feng, X.; Zhai, Q.; Wang, H.; Jiang, H.; Ren, Y. Metal–Organic Framework Surface Functionalization Enhancing the Activity and Stability of Palladium Nanoparticles for Carbon–Halogen Bond Activation. *Inorg Chem* **2022**, *61* (18), 6995–7004. https://doi.org/10.1021/acs.inorgchem.2c00379.
(35) Dong, X.; Xin, C.; Wang, L.; Gong, H.; Chen, Y. The Hydroformylation of 1-Butene on Phosphine Modified 1Rh/MOF-5 Prepared by Different Immobilization Strategies. *Molecular Catalysis* **2023**, *538*, 112973. https://doi.org/10.1016/j.mcat.2023.112973.
(36) Moiseev, D. V.; James, B. R. Phospha-Mannich Reactions of RPH2 , R2PH, and R3P. *Phosphorus Sulfur Silicon Relat Elem* **2022**, *197* (4), 327–391. https://doi.org/10.1080/10426507.2022.2036149.
(37) Mkhalid, I. A. I.; Barnard, J. H.; Marder, T. B.; Murphy, J. M.; Hartwig, J. F. C−H Activation for the Construction of C−B Bonds. *Chem Rev* **2010**, *110* (2), 890–931. https://doi.org/10.1021/cr900206p.
(38) Bisht, R.; Haldar, C.; Hassan, M. M. M.; Hoque, M. E.; Chaturvedi, J.; Chattopadhyay, B. Metal-Catalysed C–H Bond Activation and Borylation. *Chem Soc Rev* **2022**, *51* (12), 5042–5100. https://doi.org/10.1039/D1CS01012C.
(39) Wittmann, T.; Siegel, R.; Reimer, N.; Milius, W.; Stock, N.; Senker, J. Enhancing the Water Stability of Al-MIL-101-NH2 via Postsynthetic Modification. *Chemistry – A European Journal* **2015**, *21* (1), 314–323. https://doi.org/10.1002/chem.201404654.
(40) Bonnefoy, J.; Legrand, A.; Quadrelli, E. A.; Canivet, J.; Farrusseng, D. Enantiopure Peptide-Functionalized Metal–Organic Frameworks. *J Am Chem Soc* **2015**, *137* (29), 9409–9416. https://doi.org/10.1021/jacs.5b05327.
(41) Férey, G.; Mellot-Draznieks, C.; Serre, C.; Millange, F.; Dutour, J.; Surblé, S.; Margiolaki, I. A Chromium Terephthalate-Based Solid with Unusually Large Pore Volumes and Surface Area. *Science (1979)* **2005**, *309* (5743), 2040–2042. https://doi.org/10.1126/science.1116275.
(42) Kawamorita, S.; Ohmiya, H.; Hara, K.; Fukuoka, A.; Sawamura, M. Directed Ortho Borylation of Functionalized Arenes Catalyzed by a Silica-Supported Compact

Phosphine−Iridium System. *J Am Chem Soc* **2009**, *131* (14), 5058–5059. https://doi.org/10.1021/ja9008419.
(43) Yamazaki, K.; Kawamorita, S.; Ohmiya, H.; Sawamura, M. Directed Ortho Borylation of Phenol Derivatives Catalyzed by a Silica-Supported Iridium Complex. *Org Lett* **2010**, *12* (18), 3978–3981. https://doi.org/10.1021/ol101493m.
(44) Kawamorita, S.; Ohmiya, H.; Sawamura, M. Ester-Directed Regioselective Borylation of Heteroarenes Catalyzed by a Silica-Supported Iridium Complex. *J Org Chem* **2010**, *75* (11), 3855–3858. https://doi.org/10.1021/jo100352b.
(45) Konishi, S.; Kawamorita, S.; Iwai, T.; Steel, P. G.; Marder, T. B.; Sawamura, M. Site-Selective C–H Borylation of Quinolines at the C8 Position Catalyzed by a Silica-Supported Phosphane–Iridium System. *Chem Asian J* **2014**, *9* (2), 434–438. https://doi.org/10.1002/asia.201301423.
(46) Falivene, L.; Credendino, R.; Poater, A.; Petta, A.; Serra, L.; Oliva, R.; Scarano, V.; Cavallo, L. SambVca 2. A Web Tool for Analyzing Catalytic Pockets with Topographic Steric Maps. *Organometallics* **2016**, *35* (13), 2286–2293. https://doi.org/10.1021/acs.organomet.6b00371.
(47) He, J.; Bohnsack, A. M.; Waggoner, N. W.; Dunning, S. G.; Lynch, V. M.; Kaska, W. C.; Humphrey, S. M. 1-D and 2-D Phosphine Coordination Materials Based on a Palladium(II) PCP Pincer Metalloligand. *Polyhedron* **2018**, *143*, 149–156. https://doi.org/10.1016/j.poly.2017.09.025.
(48) Clavier, H.; Nolan, S. P. Percent Buried Volume for Phosphine and N-Heterocyclic Carbene Ligands: Steric Properties in Organometallic Chemistry. *Chemical Communications* **2010**, *46* (6), 841–861. https://doi.org/10.1039/b922984a.
(49) Ma, M.; Gross, A.; Zacher, D.; Pinto, A.; Noei, H.; Wang, Y.; Fischer, R. A.; Metzler-Nolte, N. Use of Confocal Fluorescence Microscopy to Compare Different Methods of Modifying Metal–Organic Framework (MOF) Crystals with Dyes. *CrystEngComm* **2011**, *13* (8), 2828–2832. https://doi.org/10.1039/c0ce00416b.
(50) Ishiyama, T.; Takagi, J.; Ishida, K.; Miyaura, N.; Anastasi, N. R.; Hartwig, J. F. Mild Iridium-Catalyzed Borylation of Arenes. High Turnover Numbers, Room Temperature Reactions, and Isolation of a Potential Intermediate. *J Am Chem Soc* **2002**, *124* (3), 390–391. https://doi.org/10.1021/ja0173019.
(51) Preshlock, S. M.; Ghaffari, B.; Maligres, P. E.; Krska, S. W.; Maleczka, R. E.; Smith, M. R. High-Throughput Optimization of Ir-Catalyzed C–H Borylation: A Tutorial for Practical Applications. *J Am Chem Soc* **2013**, *135* (20), 7572–7582. https://doi.org/10.1021/ja400295v.
(52) Syed, Z. H.; Chen, Z.; Idrees, K. B.; Goetjen, T. A.; Wegener, E. C.; Zhang, X.; Chapman, K. W.; Kaphan, D. M.; Delferro, M.; Farha, O. K. Mechanistic Insights into C–H Borylation of Arenes with Organoiridium Catalysts Embedded in a Microporous Metal–Organic Framework. *Organometallics* **2020**, *39* (7), 1123–1133. https://doi.org/10.1021/acs.organomet.9b00874.
(53) Ros, A.; Fernández, R.; Lassaletta, J. M. Functional Group Directed C–H Borylation. *Chem. Soc. Rev.* **2014**, *43* (10), 3229–3243. https://doi.org/10.1039/C3CS60418G.
(54) Chattopadhyay, B.; Dannatt, J. E.; Andujar-De Sanctis, I. L.; Gore, K. A.; Maleczka, R. E.; Singleton, D. A.; Smith, M. R. Ir-Catalyzed Ortho-Borylation of Phenols Directed by Substrate–Ligand Electrostatic Interactions: A Combined Experimental/in Silico Strategy for Optimizing Weak Interactions. *J Am Chem Soc* **2017**, *139* (23), 7864–7871. https://doi.org/10.1021/jacs.7b02232.
(55) Suresh, K.; Kalenak, A. P.; Sotuyo, A.; Matzger, A. J. Metal-Organic Framework (MOF) Morphology Control by Design. *Chemistry – A European Journal* **2022**, *28* (18), e202200334. https://doi.org/10.1002/chem.202200334.
(56) Uson, R.; Oro, L. A.; Cabeza, J. A.; Bryndza, H. E.; Stepro, M. P. Dinuclear Methoxy, Cyclooctadiene, and Barrelene Complexes of Rhodium(I) and Iridium(I). In *Inorganic Syntheses*; 1985; Vol. 23, pp 126–130. https://doi.org/10.1002/9780470132548.ch25.
(57) Bührmann, M.; Hardick, J.; Weisner, J.; Quambusch, L.; Rauh, D. Covalent Lipid Pocket Ligands Targeting P38α MAPK Mutants. *Angewandte Chemie International Edition* **2017**, *56* (43), 13232–13236. https://doi.org/10.1002/anie.201706345.
(58) Rouquerol, J.; Llewellyn, P.; Rouquerol, F. Is the BET Equation Applicable to Microporous Adsorbents? *Stud Surf Sci Catal* **2007**, *160*, 49–56. https://doi.org/10.1016/S0167-2991(07)80008-5.
(59) Walton, K. S.; Snurr, R. Q. Applicability of the BET Method for Determining Surface Areas of Microporous Metal−Organic Frameworks. *J Am Chem Soc* **2007**, *129* (27), 8552–8556. https://doi.org/10.1021/ja071174k.
(60) Hartmann, M.; Fischer, M. Amino-Functionalized Basic Catalysts with MIL-101 Structure. *Microporous and Mesoporous Materials* **2012**, *164*, 38–43. https://doi.org/10.1016/j.micromeso.2012.06.044.
(61) Moiseev, D. V.; Marcazzan, P.; James, B. R. Reversible Decomposition of Mono(α-Hydroxy)Phosphines and Their Reaction with α,β-Unsaturated Aldehydes. *Can J Chem* **2009**, *87* (4), 582–590. https://doi.org/10.1139/V09-021.
(62) *Ohio Supercomputer Center: Columbus, OH*. http://www.osc.edu/ (accessed 2021-06-08).

Table of Contents Graphic: